

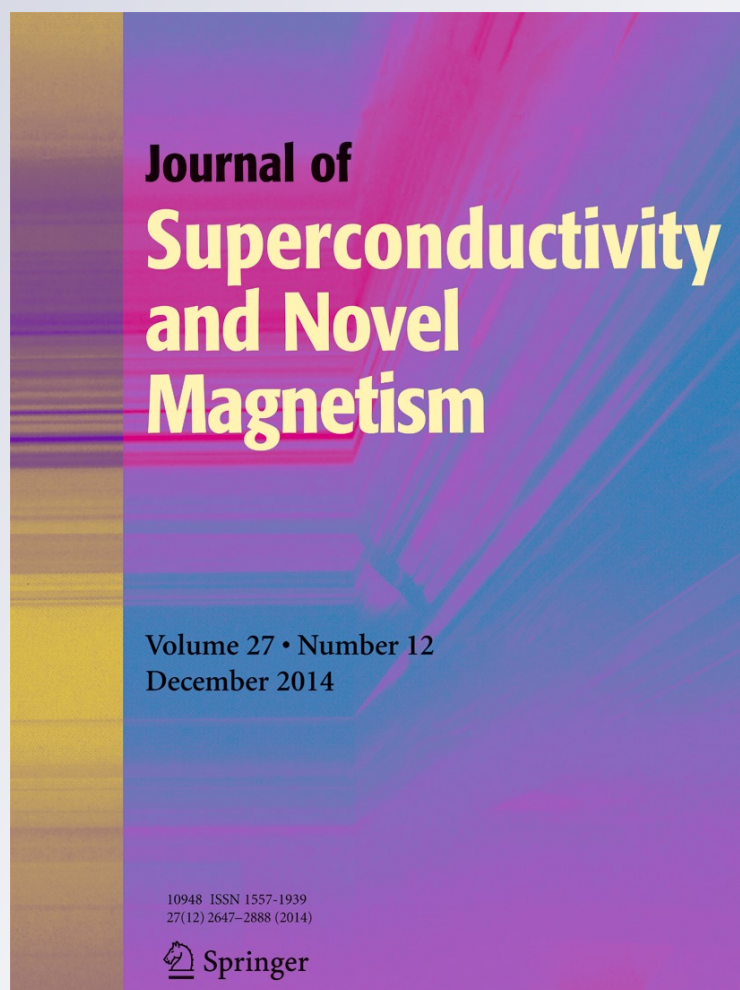
# *Synthesis of Superparamagnetic Nanoparticle $Ni_{0.50}Zn_{0.50}Fe_2O_4$ Using Wet Chemical Method*

**Manoj M. Kothawale, Rajesh Pednekar & Sher Singh Meena**

**Journal of Superconductivity and Novel Magnetism**  
Incorporating Novel Magnetism

ISSN 1557-1939  
Volume 27  
Number 12

J Supercond Nov Magn (2014)  
27:2829-2833  
DOI 10.1007/s10948-014-2769-8



**Your article is protected by copyright and all rights are held exclusively by Springer Science +Business Media New York. This e-offprint is for personal use only and shall not be self-archived in electronic repositories. If you wish to self-archive your article, please use the accepted manuscript version for posting on your own website. You may further deposit the accepted manuscript version in any repository, provided it is only made publicly available 12 months after official publication or later and provided acknowledgement is given to the original source of publication and a link is inserted to the published article on Springer's website. The link must be accompanied by the following text: "The final publication is available at [link.springer.com](http://link.springer.com)".**

# Synthesis of Superparamagnetic Nanoparticle $\text{Ni}_{0.50}\text{Zn}_{0.50}\text{Fe}_2\text{O}_4$ Using Wet Chemical Method

Manoj M. Kothawale · Rajesh Pednekar ·  
Sher Singh Meena

Received: 28 August 2014 / Accepted: 1 September 2014 / Published online: 16 September 2014  
© Springer Science+Business Media New York 2014

**Abstract** The nanoparticles of  $\text{Ni}_{0.50}\text{Zn}_{0.50}\text{Fe}_2\text{O}_4$  were prepared using cotton base wet chemical method. The X-ray diffraction (XRD) spectrum shows single phase cubic spinel structure, and crystallite size calculated using the Debye–Scherrer formula for 311 planes was found to be  $41 \text{ nm} \pm 5 \%$ . The nano range sizes of particle were confirmed using transmission electron microscope (TEM) and atomic force microscopy (AFM) images. The porosity value of the sample is promising towards sensor applications. Infrared spectroscopic results reveal two main absorption bands, indicating sample is having single phase spinel structure with two sublattices. The high DC resistivity of the sample is attributed to nano range particle sizes. The superparamagnetic (SPM) nature was confirmed from a variation of magnetic moment with applied magnetic field using VSM. The Mössbauer spectrum recorded at room temperature shows two major sextets corresponding to A- and B-site Fe ions. The relaxed sextet is associated with the atoms near the surface of the nanoparticles experiencing disordered spins. The central doublet in Mössbauer spectra of the sample indicates SPM particles. The isomer shift results show that all the Fe ions are in high state.

**Keywords** Ni–Zn ferrites · XRD · TEM · Superparamagnetism · Isomer shift · DC resistivity

## 1 Introduction

Spinel ferrites are technologically important for several electromagnetic devices because of their high Curie temperature, high permeability, high electrical resistivity, low eddy current, and low dielectric loss. Ni–Zn ferrites are commercially important due to their uses in devices operating at high frequency such as radio-frequency coils, transformer cores, etc. [1]. The properties of ferrite are sensitive to method of preparation, compositions, particle sizes, and size distribution [2]. In the present work, nanoparticles of  $\text{Ni}_{0.50}\text{Zn}_{0.50}\text{Fe}_2\text{O}_4$  were prepared using cotton base wet chemical method. Properties such as particle sizes, saturation magnetization, DC electrical resistivity, porosity, and Mossbauer hyperfine parameters were studied.

## 2 Experimental

Calculated amount of ferric nitrate, nickel nitrate, and zinc nitrate (all salts of AR grade) in stoichiometry proportions were dissolved in the minimum amount of distilled water. This solution was soaked using the optimum amount of cotton. The soaked cotton pieces were placed in crucible and heated in conventional box-type furnace for 6 h at  $600^\circ\text{C}$ . The decomposition of soaked solution resulted into fine powder of Ni–Zn ferrite. The powder obtained was used for characterization. The X-ray powder diffraction pattern was recorded on Rigaku X-ray diffractometer using  $\text{CuK}\alpha$  radiation and  $2\theta$  scanning range from  $20^\circ$  to  $80^\circ$ . IR spectrum

---

M. M. Kothawale (✉)

Department of Physics, DM's College of Arts, Science and Commerce, Assagao, Goa 403507, India  
e-mail: manojkothawale@yahoo.com

R. Pednekar

Department of Chemistry, DM's College of Arts, Science and Commerce, Assagao, Bardez Goa, 403507, India

S. S. Meena

Solid State Physics Division, Physics Division, Bhabha Atomic Research Centre, Mumbai, 400085, India

of sample was recorded using a Shimadzu Fourier transform infrared (FTIR) 8900 spectrometer in the range of  $300\text{--}4000\text{ cm}^{-1}$ . The pallet was prepared with KBr to a sample ratio of 1:100 for IR measurements. Transmission electron microscope (TEM) image was recorded on Hitachi H7500. Atomic force microscopy (AFM) image was recorded on NT-MDT's Integra AFM via semicontact mode. Variation of magnetic moment at room temperature was recorded using VSM (Lakeshore model 7404) up to a field of 2 T, and corresponding hysteresis curve was obtained. The room temperature Mössbauer spectrum of the sample was recorded in constant acceleration mode using a  $^{57}\text{Co}$ . The calibration of the velocity scale was done using  $^{57}\text{Fe}$  metal foil. Mass density was calculated using the Archimedes principle [3]. The freshly prepared powder was pressed into pellet (10 mm dia and 2 mm thick) by applying pressure of 75 kN for 5 min. The pellet was then coated with silver on both surfaces for having good electrical contact. The DC resistivity was measured by a two-probe method using the Keithley electrometer in the temperature range of 30 to 500 °C in steps of 5 °C.

### 3 Results and Discussion

#### 3.1 X-ray Diffraction, TEM, and AFM Analysis

The X-ray diffraction (XRD) pattern of the sample is shown in Fig. 1. The strongest reflection from (311) plane denotes the spinel phase. The positions of peaks comply with reported JCPDS file no. 8-234. This confirms that sample under study is having single phase cubic spinel structure. The observed lattice constant value of 8.3977 (Å) is comparable with reported literature [1].

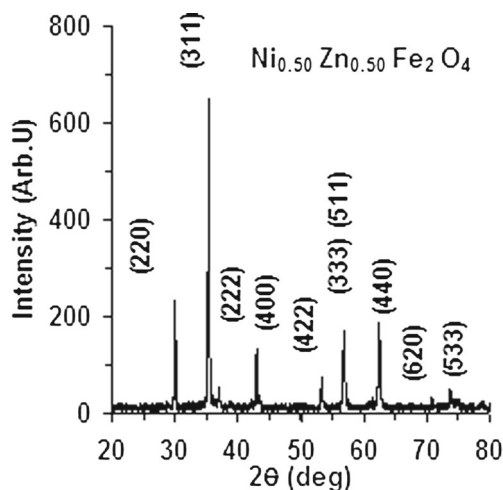


**Fig. 1** XRD pattern of  $\text{Ni}_{0.50}\text{Zn}_{0.50}\text{Fe}_2\text{O}_4$

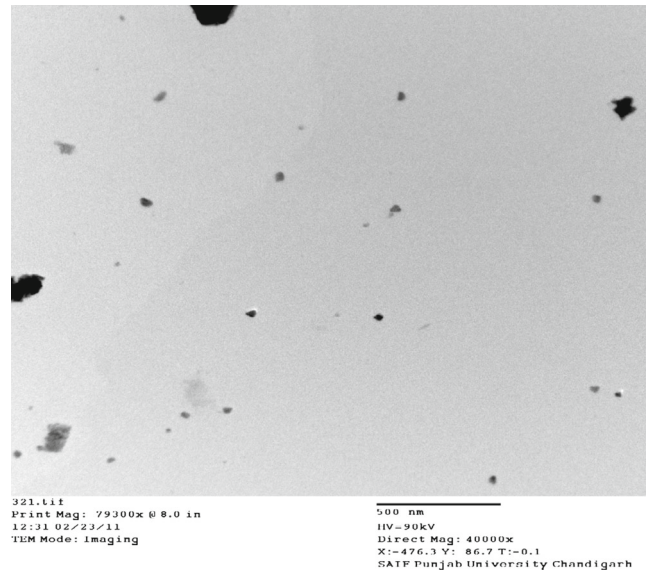


**Fig. 2** TEM image of  $\text{Ni}_{0.50}\text{Zn}_{0.50}\text{Fe}_2\text{O}_4$

The crystallite size of a nanocrystalline sample for 311 planes was calculated using the Debye–Scherrer formula given in (1).

$$D = 0.89\lambda / \beta \cos \theta \quad (1)$$

where  $D$  is the crystallite size in nanometers,  $\lambda$  is the X-ray wavelength in angstrom,  $\beta$  is the line broadening at full width half maximum intensity (FWHM) in radians, and  $\theta$  is the Bragg angle. The crystallite size was found to be  $41\text{ nm} \pm 5\%$ .

The TEM image of the sample is shown in Fig. 2. The particle sizes vary in the range of 15 to 64 nm. The AFM image of the sample in Fig. 3 shows that particle sizes vary in the large range of 20 to 80 nm. The porosity of the sample was found to be  $24 \pm 5\%$ .

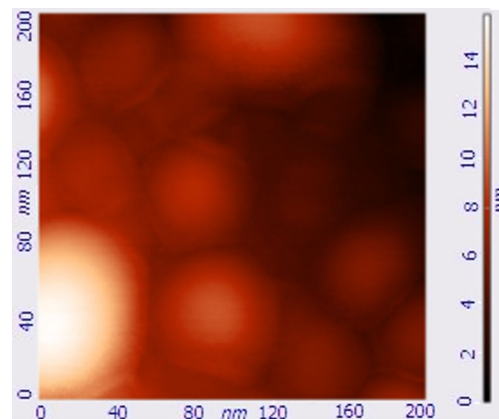


**Fig. 3** AFM image of  $\text{Ni}_{0.50}\text{Zn}_{0.50}\text{Fe}_2\text{O}_4$

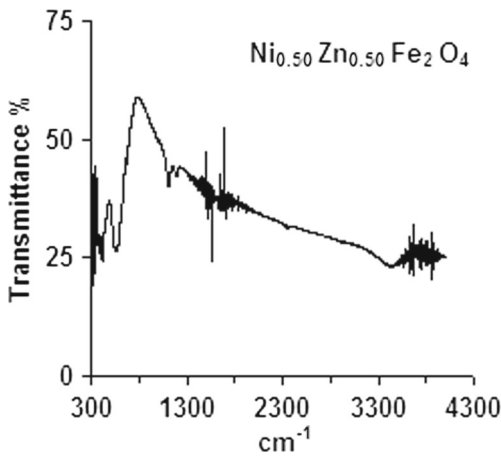


Fig. 4 IR spectrum of  $\text{Ni}_{0.50}\text{Zn}_{0.50}\text{Fe}_2\text{O}_4$

### 3.2 IR Analysis

The IR absorption spectrum of sample show two absorption bands as can be seen in Fig. 4. The higher band  $\nu_1$  is between wave numbers 600 and 550  $\text{cm}^{-1}$  whereas lower band  $\nu_2$  between 450 and 385  $\text{cm}^{-1}$ . This is a common feature of all the ferrites indicating single phase spinel structure having two sub-lattices [4–7]. The highest band corresponds to intrinsic stretching vibrations of metals at the tetrahedral site, whereas the lowest band is assigned to octahedral metal stretching.

### 3.3 DC Resistivity

The plot of  $\log \rho$  vs.  $1000/T$  of the sample is shown in Fig. 5. It can be seen that the DC resistivity decreases with increasing temperature showing typical semiconductor-like behavior. The variation in resistivity curve can be divided into three temperature regions. Region (I) is in the relatively lower temperature range up to 400 K ( $\sim 125^\circ\text{C}$ ). In this region, resistivity does not exhibit much variation with temperature. The conduction phenomenon in this region is

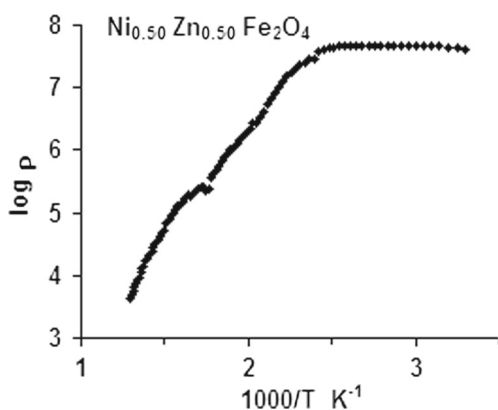


Fig. 5  $\log \rho$  vs.  $1000/T$  of  $\text{Ni}_{0.50}\text{Zn}_{0.50}\text{Fe}_2\text{O}_4$

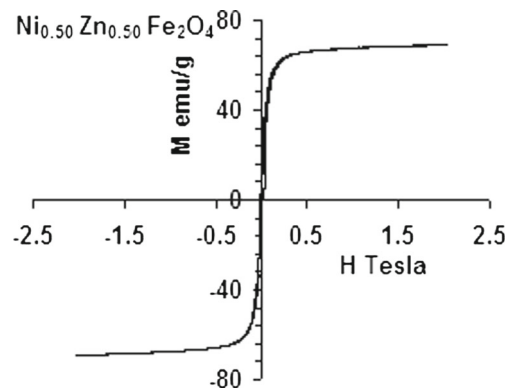


Fig. 6  $M-H$  loop of  $\text{Ni}_{0.50}\text{Zn}_{0.50}\text{Fe}_2\text{O}_4$  at room temperature

mostly attributed to scattering of charge carriers by lattice vibrations, impurities in the sample, presence of lattice defects (defects are having smaller mobility), voids, and high resistive grain boundaries or existence of resonant phonon modes [8].

The region (II) was observed in the temperature range around 400 to 675 K ( $125$  to  $400^\circ\text{C}$ ). In this region, resistivity decreases with increase in temperature and the conduction phenomenon is attributed to the thermally activated mobility of the charge carriers. The change in slope of the curve was also found in this region. The small dip or cusps in the curves causing change in the slope can be clearly seen. This change is related to the magnetic transition from ferrimagnetic to paramagnetic state and corresponding temperature to the Curie point ( $T_C$ ) of the sample [9]. In region (III) for temperature range  $T > 673$  K ( $400^\circ\text{C}$ ), the resistivity decreases rapidly with temperature (above  $T_C$ ). This decrease in resistivity is mainly associated to the increase

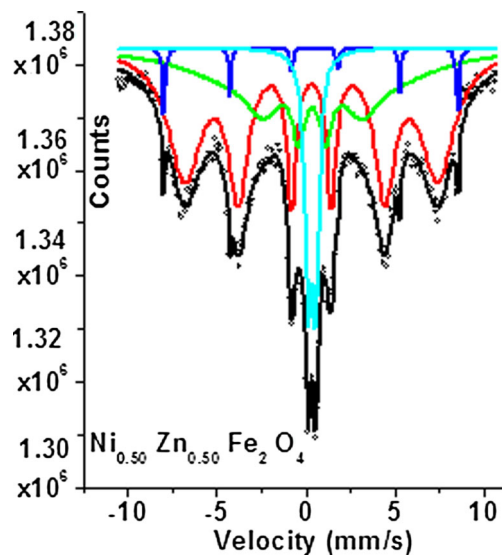


Fig. 7 Mössbauer spectrum of  $\text{Ni}_{0.50}\text{Zn}_{0.50}\text{Fe}_2\text{O}_4$

**Table 1** The isomer shift ( $\delta$ ), quadrupole splitting ( $\Delta$ ), hyperfine field values ( $H$ ), outer line width ( $T$ ) and areas in percentage of tetrahedral (A) and octahedral (B) sites occupied by  $\text{Fe}^{3+}$  ions of  $\text{Ni}_{0.50}\text{Zn}_{0.50}\text{Fe}_2\text{O}_4$  sample derived from Mössbauer spectra recorded at room temperature

Parameters	Iron site			Doublet
	A	B	C	
Hyperfine field, $H$ (T)	44.13	51.23	29.62	–
Isomer shift ( $\delta$ ) mm/s	0.311	0.490	0.352	0.335
Quadrupole splitting, $\Delta$ (mm/s)	0.003	0.111	0.018	0.433
Outer line width, $T$ (mm/s)	2.240	0.185	6.556	0.423
Area %	56.20	2.43	31.36	10.01

[Isomer shift values are relative to  $\alpha\alpha$ -Fe (0.00 mm/s) foil]

in thermally activated drift mobility of the charge carriers in accordance with the hopping conduction model [10]. The higher-temperature region above  $T_C$  is corresponding to a paramagnetic disordered region with comparatively high activation energy. The room temperature resistivity of nano samples is of the order of  $6.5 \times 10^7$  ohm/cm.

### 3.4 $M - H$ Loop

The variation of magnetization ( $M$ ) with the static applied magnetic field ( $H$ ) (up to 2 T) at room temperature is shown in Fig. 6. The magnetization increases with increasing applied magnetic field and attains its saturation value for fields higher than 0.50 T. The saturation magnetization was found to be 68 emu/g. The close hysteresis loop observed at room temperature indicates superparamagnetic (SPM) nature of nanoparticles.

### 3.5 Mössbauer Spectrum

The room temperature Mössbauer spectrum recorded to monitor the local environment around Fe cations is shown in Fig. 7. The solid line in Fig. 7 represents the simulated curves, whereas solid circles represent experimental data points. Each spectrum was fitted with the three magnetic sextets which are arising due to Zeeman splitting. The two major sextets are corresponding to Fe ions residing at the A site (inner sextet) and B site (outer sextet) of the lattices. This is an indication of ferrimagnetic behavior of the samples [11]. The observed six-line magnetic patterns in the spectra are attributed to super exchange interaction between the magnetic ions at A and B sub-lattices.

The third broad featureless absorption sextet characterized by a significant reduction of the magnetic hyperfine field is associated with relaxation effect. The Fe ions corresponding to broad sextet with much smaller hyperfine field than that of major sextet may be associated with the atoms near the surface of the nanoparticles experiencing disordered spins [12]. This relaxation effect may also be due to

the presence of strong interparticle interactions and nano sizes of particles of the samples [13]. The area of this broad sextet may be associated with the range of nanoparticles. The appearance of central doublet is indicating the presence of SPM particles in the sample. The various Mössbauer parameters of sample are given in Table 1. The results of the isomer shift vary in the range of 0.311 to 0.490 mm/s. This shows that Fe ions are in the trivalent state. The quadrupole shift ( $\Delta\Delta$ ) values were found to be low and is indicating that the local symmetry of the magnetic phase of A sites is close to cubic, while that of B site is close to trigonal [14, 15].

## 4 Conclusions

The nanoparticles of  $\text{Ni}_{0.5}\text{Zn}_{0.5}\text{Fe}_2\text{O}_4$  were successfully synthesized by simple and easy cotton base wet chemical method. The crystallite size calculated using X-ray spectra is comparable with particle sizes obtained from TEM and AFM images. The high DC resistivity at room temperature is attributed to nano sizes of particles. The sample show high saturation magnetization and superparamagnetic nature at room temperature. The Fe ions at the A and B sites are in trivalent state. The detailed dielectric studies can be undertaken in the future.

**Acknowledgments** The author is thankful to UGC, New Delhi, for granting the Minor Research Project.

## References

- Jadhav, S.S., Shirsath, S.E., Toksha, B.G., Shukla, S.J., Jadhav, K.M.: Chin. J. Chem. Phys. **21**, 381–386 (2008)
- Mahmud, S.T., Akther Hossain, A.K.M., Abdul Hakim, A.K.M., Seki, M., Kawai, T., Tabata, H.: J. Magn. Magn. Mater. **305**, 269–274 (2006)
- Sheikh, A.D., Mathe, V.L.: J. Mater. Sci. **43**, 2018–2025 (2008)
- Akther Hossain, A.K.M., Mahmuda, S.T., Seki, M., Kawai, T., Tabata, H.: J. Magn. Magn. Mater. **312**, 210–219 (2007)

5. Ayer, R., Desai, R., Upadhyay, R.V.: *Bull. Mater. Sci.* **32**, 141–147 (2009)
6. Ayer, R., Desai, R., Upadhyay, R.V.: *Indian J. Pure Appl. Phys.* **47**, 180–185 (2009)
7. Ladgaonkar, B.P., Kolekar, C.B., Vaingankar, A.S.: *Bull. Mater. Sci.* **25**, 351–358 (2002)
8. El-Sayed, A.M.: *Mater. Chem. Phys.* **82**, 583–587 (2003)
9. Srinivasan, T.T., Ravindranathan, P., Cross, L.E., Roy, R., Newman, R.E., Sankar, S.G., Patil, K.C.: *J. Appl. Phys.* **63**, 3789–3794 (1988)
10. Bhosale, A.G., Chougule, B.K.: *Mater. Lett.* **60**, 3912–3915 (2006)
11. Dhiman, R.L., Taneja, S.P., Reddy, V.R.: *Ad. Cond. Matt. Phys.*, 1–7 (2008)
12. Singh, L.H., Govindaraj, R., Amarendra, G., Sundar, C.S.: *AIP Conf. Proc.* **1447**, 445–446 (2012). doi:[10.1063/1.4710071](https://doi.org/10.1063/1.4710071)
13. Albuquerque, A.S., Ardisson, J.D., Waldemar, A.A.M., Alves, M.: *J. Appl. Phys.* **87**, 4352–4357 (2000)
14. Attia, S.M.: *Egypt. J. Solids* **29**(2), 329–339 (2006)
15. Blasko, J., Garcia, J.: *Phys. Rev. B* **83**, 104–105 (2011)